AIP Advances

Atomistic tensile deformation mechanisms of Fe with gradient nano-grained structure

Wenbin Li, Fuping Yuan, and Xiaolei Wu

Citation: AIP Advances **5**, 087120 (2015); doi: 10.1063/1.4928448
View online: http://dx.doi.org/10.1063/1.4928448
View Table of Contents: http://scitation.aip.org/content/aip/journal/adva/5/8?ver=pdfcov
Published by the AIP Publishing

Atomistic tensile deformation mechanisms of Fe with gradient nano-grained structure

Wenbin Li,[a] Fuping Yuan,[b] and Xiaolei Wu[a]
State Key Laboratory of Nonlinear Mechanics, Institute of Mechanics, Chinese Academy of Science, No.15, North 4th Ring, West Road, Beijing 100190, People's Republic of China

(Received 25 May 2015; accepted 29 July 2015; published online 6 August 2015)

Large-scale molecular dynamics (MD) simulations have been performed to investigate the tensile properties and the related atomistic deformation mechanisms of the gradient nano-grained (GNG) structure of bcc Fe (gradient grains with d from 25 nm to 105 nm), and comparisons were made with the uniform nano-grained (NG) structure of bcc Fe (grains with d = 25 nm). The grain size gradient in the nano-scale converts the applied uniaxial stress to multi-axial stresses and promotes the dislocation behaviors in the GNG structure, which results in extra hardening and flow strength. Thus, the GNG structure shows slightly higher flow stress at the early plastic deformation stage when compared to the uniform NG structure (even with smaller grain size). In the GNG structure, the dominant deformation mechanisms are closely related to the grain sizes. For grains with d = 25 nm, the deformation mechanisms are dominated by GB migration, grain rotation and grain coalescence although a few dislocations are observed. For grains with d = 54 nm, dislocation nucleation, propagation and formation of dislocation wall near GBs are observed. Moreover, formation of dislocation wall and dislocation pile-up near GBs are observed for grains with d = 105 nm, which is the first observation by MD simulations to our best knowledge. The strain compatibility among different layers with various grain sizes in the GNG structure should promote the dislocation behaviors and the flow stress of the whole structure, and the present results should provide insights to design the microstructures for developing strong-and-ductile metals. [http://dx.doi.org/10.1063/1.4928448]

I. INTRODUCTION

Nano-grained (NG) metals usually have ultra-high strength, but show reduced strain hardening rate and limited ductility compared to their coarse grained (CG) counterparts, due to the incapability of effectively accumulating dislocations inside the nano-grains.[1–3] The structural applications in modern industry always demand stronger and tougher metals and alloys. Such expectations have been realized by several strategies developed recently through tailoring nano-scale microstructures, such as, pre-existing growth nano-twins, nano-precipitates, bimodal grain size distribution, and gradient nano-grained (GNG) structure.[4–16]

The GNG/CG architecture, consisting of the GNG surface layers and the CG core, can produce high strength and ductility.[11–16] Based on surface nanocrystallization and warm co-rolling technologies, high strength and exceptional ductility could be obtained in the periodically layered GNG/CG structures by introducing non-localized fracture behaviors.[12] High tensile plasticity can also be achieved in the NG Cu film when confined by a CG substrate with a gradient grain size transition, which attributes largely to a mechanically-driven grain boundary migration process and a

[a]liwenbin0115@163.com and xlwu@imech.ac.cn
[b]Corresponding author. Tel: +86-10-82544409; fax: +86-10-82543977; E-mail address: fpyuan@lnm.imech.ac.cn

strain-induced growth of nano-grains[13] where strain localization is suppressed.[17,18] Evidences have been indicated that large plastic strains could be obtained in NG metals without apparent grain growth by other deformation modes, such as compression and rolling,[19–21] in which complex stress states exist in the specimens instead of uniaxial stress state. These experimental observations hint that a stable GNG layer may also intrinsically improve ductility without grain growth, and the strain compatibility between different layers may suppress the strain localization of the NG surface layers for improved ductility, as indicated in our previous work.[14] The strain compatibility between different layers usually induces stress partitioning, stress state change and back stress in the GNG structure, and the back stress usually refers to the stress associated with a strain process providing long-range interactions with mobile dislocations (such as geometrically necessary dislocations, GNDs) for back stress hardening.[22] The generation of GNDs increases the dislocation density in the materials and makes it more likely for dislocations to interact and entangle with each other, which increases the flow stress.[14,23,24] Moreover, the strain gradient should be introduced when the constraint exists, which produces the extra hardening and the higher strength compared to the rule-of-mixture due to the grain size gradient.[14,24,25]

Nanocrystalline (NC) bcc metals have been found to behave very differently from NC metals with other crystal structures.[26–28] With decreasing grain size, the density of mixed and edge dislocations increases while the screw dislocations become less dominated for bcc metals.[27] Moreover, the overall dislocation density decreases with decreasing grain size when the grain sizes are very small.[27] The strain rate sensitivity was found to decrease with decreasing grain size for bcc metals due to these observations.[26–28] MD simulations have been shown to be particularly helpful for investigating the atomistic deformation mechanisms of nanostructured metals, in which the real-time microstructural responses of the system, the atomistic and macroscopic stress and strain, and the stress state can be examined in detail.[7,29–41] For example, previous investigations[29,30,36,39] have elucidated a transition in the dominant deformation mechanisms with decreasing grain size from dislocation-mediated plasticity to GB-associated plasticity in NC metals. Previous MD simulations on bcc Fe have also indicated that the type of dislocations is full lattice dislocation even when the grain size is below 20 nm.[33,39–41] The fracture resistance of bcc NC Fe has been shown to increase with decreasing grain size below a critical grain size, and the "most brittle grain size" appears to be in accordance with the "strongest grain size".[33] MD simulations have also been used to characterize the dislocation-core structure in the framework of the Peierls-Nabarro model and study the mechanism of the dislocation motion at different temperatures in bcc Fe.[40] The dislocations were found to move by nucleation and propagation of kink-pairs along its line at low temperature.

MD simulations may be helpful and provide hints for the atomistic tensile deformation mechanisms in the GNG structure. In this regard, large-scale MD simulations were utilized in this work to investigate and compare the tensile properties and the related atomistic deformation mechanisms of two microstructures, i.e., the GNG structure of bcc Fe and the uniform NG structure of bcc Fe.

II. SIMULATION TECHNIQUES

The MD simulations were carried out using the Large-scale Atomic/Molecular Massively Parallel Simulator (LAMMPS) code and the force interactions between atoms were described by an Fe EAM potential developed by Mendelev *et al*.[42] This potential was calibrated according to the *ab initio* values or the experimental data of lattice constant, elastic constants, point-defect energies, bcc-fcc transformation energy, and relaxed core structure of the dislocations. In order to explore deformation mechanisms of GNG structure, similar to the configuration used by Yamakov *et al*.,[29] a columnar grain structure was considered in which grains larger than those possible in fully 3-dimensional simulations could be simulated. The <111> direction was chosen for the column axis (z direction) in the present study, which ensures that dislocations can glide on either of three {110} slip systems in each grain following their nucleation. In this study, two configurations were considered, i.e., the GNG structure of bcc Fe and the uniform NG structure of bcc Fe. The relaxed structures for these two configurations are shown in Fig. 1, and the color coding is based on the common neighbor analysis (CNA) values. Green color stands for perfect bcc atoms, red color stands for grain boundaries (GBs), dislocation core, and free surface atoms, blue color stands for fcc atoms, pink color stands for hcp

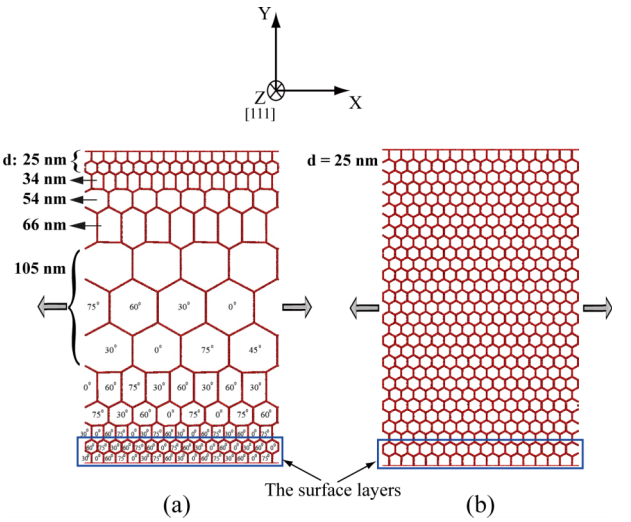

FIG. 1. The relaxed tensile configurations for (a) GNG structure of bcc Fe; (b) uniform NG structure of bcc Fe. Perfect bcc atoms are not shown in this figure.

atoms. The same CNA color coding is used in all figures of present study. In Fig. 1(a), a GNG structure of 140 grains with various orientations was constructed by the Voronoi method, and the grain size increases gradually from 25 nm at the surface to 105 nm at the center. In Fig. 1(b), a uniform NG structure of 464 grains with various orientations was also constructed by the Voronoi method. In Fig. 1, the x direction is along $[11\bar{2}]$ and the y direction is along $[1\bar{1}0]$ for the grain with 0 angle, and the grains with other angles were rotated about the z axis from this reference grain. Both configurations are symmetric about the center line along y direction. The surface layers have the same grain sizes, structures and orientations for both configurations, as shown in Fig. 1. Both samples have dimensions of $400 \times 650 \times 0.99$ nm^3, and contain approximately 24,000,000 atoms. The thickness (0.99 nm) of the columnar grains was chosen to be larger than the cutoff distance (0.53 nm) of the EAM interatomic potential in order to ensure the periodicity along the z direction. Unlike the bowed-out dislocations with curvature from GBs of real nanocrystals, vertical GBs of an ideal columnar structure normally produce infinite straight dislocations, however previous research[7,29] have indicated that such simulation structure can also provide insights for atomistic deformation mechanisms of nanostructured metals with proper orientation selection. Periodic boundary conditions were imposed along x and z directions, while free boundary conditions were imposed along y directions. Both as-created samples were first subjected to energy minimization using the conjugate gradient method before tensile loading, then gradually heated up to the desired temperature and finally relaxed in the Nose/Hoover isobaric-isothermal ensemble (NPT) under both the pressure 0 bar and the desired temperature (1K) for enough time (100 ps). After relaxation, an 8% strain was applied to both samples with a constant engineering strain rate of $2 \times 10^8 s^{-1}$ along x direction. During the tensile loading, the overall pressures in the y and z directions were kept to zero.

III. RESULTS AND DISCUSSIONS

In the GNG/CG sandwich samples produced by the surface mechanical attrition treatment (SMAT) or the surface mechanical grinding treatment (SMGT),[11–14] the gradient layer generally has gradient grain sizes along the depth from several tens of nm to several tens of μm. Under uniaxial tension, the outer NG layers will first become plastically unstable at lower tensile strains, resulting in fast lateral shrinking of unstable layers. However, the lateral shrinking is constrained and stopped by the neighboring stable large-grained layer since the strain compatibility is required to maintain material continuity. Moreover, the constraint induces the lateral tensile stress in the NG layers and the lateral compressive stress in the inner layers.[14]

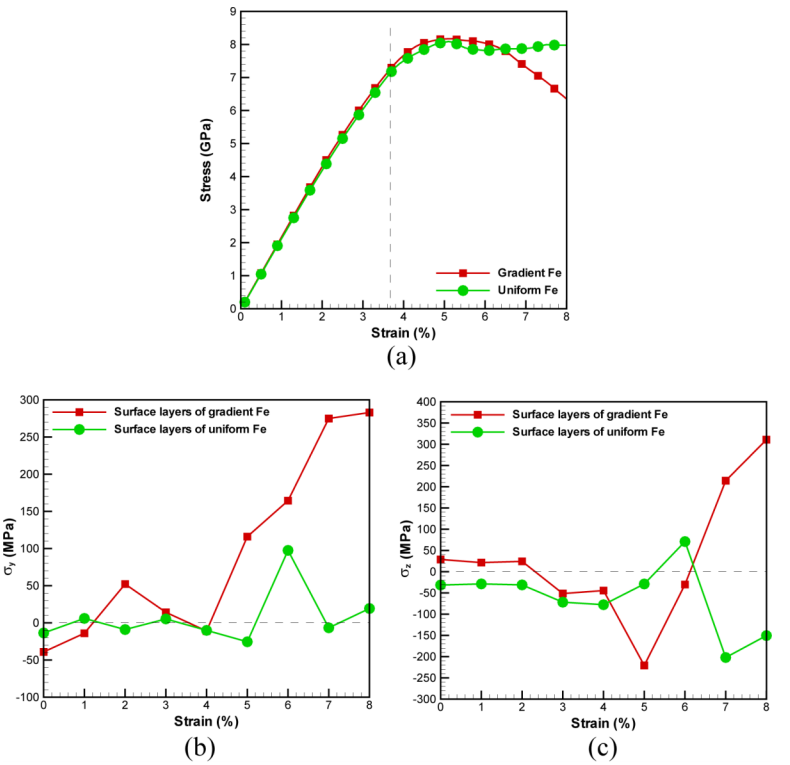

FIG. 2. (a) Simulated stress (σ_x) as a function of tensile strain for both configurations; (b) Simulated lateral stress σ_y as a function of tensile strain for the surface layers in both configurations; (c) Simulated lateral stress σ_z as a function of tensile strain for the surface layers in both configurations.

In our simulation model of the GNG structure, the gradient grain size transition is only from 25 nm at the surface to 105 nm at the center due to the computation limitations of MD simulations. However, the stress states for both the surface layers and the center layer in the GNG sample are still observed to change from uniaxial tension to multi-axial states during the deformation, as indicated in Fig. 2. Fig. 2(a) shows simulated stress (σ_x) as a function of tensile strain for both the GNG structure and the uniform NG structure. Figs. 2(b) and 2(c) show simulated lateral stresses (σ_y and σ_z) as a function of tensile strain for the surface layers in both configurations. In Figs. 2(b) and 2(c), the lateral stresses represent the average lateral stresses based on all atoms from the surface layers in both configuration. As indicated, the constraint between the surface layers and the center layer induces lateral tensile stresses in the surface layers for the GNG structure, which is contrast to the uniform NG structure where nearly zero lateral stresses are observed in both the surface layers and the center layer. The overall lateral stresses are still zero in the GNG structure during the tensile loading (the overall lateral stresses are monitored during loading, and the overall sample is still under uniaxial loading). Correspondingly, lateral compressive stresses should be induced in the center layer since the overall pressures in the y and z directions were kept to zero for the whole GNG structure during the loading. It should be noted that free boundary condition is intended to impose on y direction like the real GNG sample, and the strain compatibility between the surface layers and the center layer may suppress the strain localization of the surface layers, which results in the stress-state change.

Fig. 3(a) shows the number of dislocations as a function of tensile strain for the surface layers in both configurations. Figs. 3(b) and 3(c) show the simulated deformation patterns of selected grains in the surface layers for the uniform NG structure and the GNG structure, respectively. The strongest grain size in bcc Fe was found to be approximately 15 nm by previous MD simulations.[39] This indicates that the 25 nm grains should be stronger than the 105 nm grains in our simulation model. However, as indicated in Fig. 2(a), the flow stress of the GNG structure (with a high volume fraction for grains with d = 105 nm) at early plastic deformation stage is comparable to and even

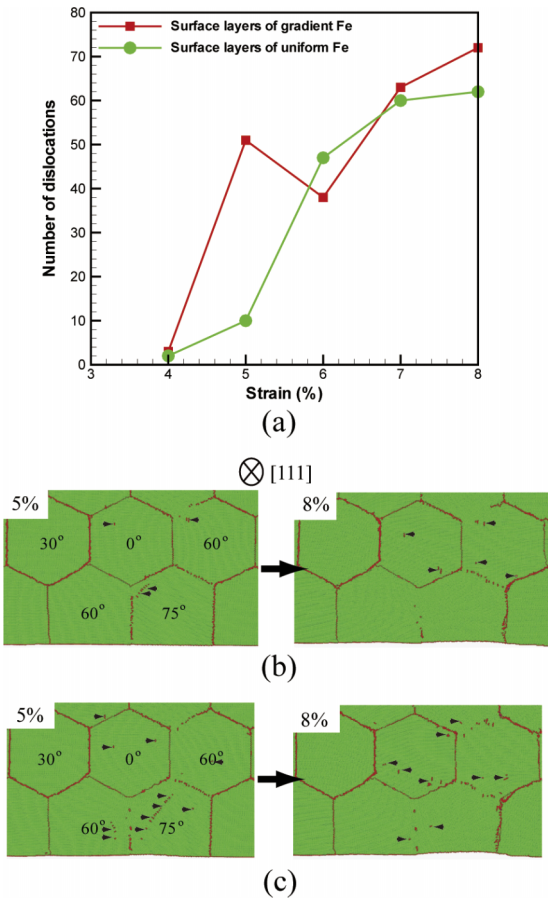

FIG. 3. (a) Number of dislocations as a function of tensile strain for the surface layers in both configurations. Simulated deformation patterns at 5% and 8% tensile strains of selected grains in the surface layers ($d = 25$ nm) for (b) the uniform NG structure of bcc Fe; (c) the GNG structure of bcc Fe.

slightly higher than that of the uniform NG structure (d = 25 nm). The underlying mechanisms should be twofold. First, the stress state change is expected to increase the dislocation density in the materials and make it more likely for dislocations to interact and entangle with each other, which increases the flow stress.[23] As indicated in Fig. 3a, higher dislocation density is observed in the GNG structure for the same surface layer due to the stress state change and the constraint, when compared to the uniform NG structure. Second, the strain gradient occurs when the constraint exists, which produces the GNDs and the extra hardening due to the grain size gradient.[14,24] Several dislocations can be observed as red dots marked by arrows within grain interiors of the surface layers for the uniform NG structure (Fig. 3b). However, as indicated in Fig. 3c, more dislocations can be found in the same grains for the GNG structures, and these dislocations seem to nucleate at GBs since there are no initial dislocation sources inside the grains.

Fig. 4 shows the overall simulated deformation patterns for the GNG structure of bcc Fe at tensile strains of 4% and 6%. A small crack is observed to nucleate at the GB of two large grains at a tensile strain of 6%, which produces a abrupt drop in the flow stress for the GNG structure as shown in the Fig. 2(a). A few dislocations are observed in the small grains (d = 25 nm). Larger number of dislocations are observed in the interiors of large grains (d = 105 nm). Moreover, as indicated later, the dominant deformation mechanisms are closely related to the grain sizes in the GNG structure.

Figs. 5(a) and 5(b) show nucleation of a dislocation from GBs and propagation of the dislocation in the interior of grains, respectively. This confirms that GBs are the sources of dislocations, and the dislocation type is full lattice dislocation. Figs. 5(c) and 5(d) show a typical edge dislocation with edge component of $1/3[\bar{1}\bar{1}2]$ projected onto [111] plane and a typical screw dislocation in the

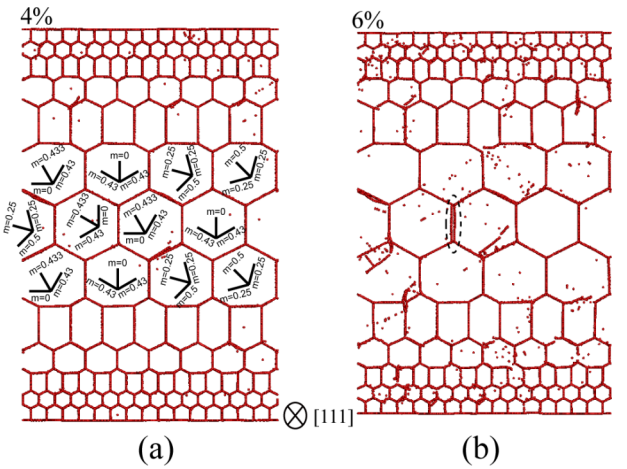

FIG. 4. The overall simulated deformation patterns for GNG structure of bcc Fe at a tensile strain of (a) 4%; (b) 6%. A small crack is observed to nucleate at GB of large grains, indicated by a dash ellipse. The Schmid Factors for three {110} slip systems in each large grain (d = 105 nm) are also indicated in Fig. 4(a).

interior of grains, respectively. Crystallographic analysis and image simulations reveal that the best way to study dislocations with edge components in bcc systems is to take images along <110> zone axis, from which it is possible to identify 1/2<111> pure edge dislocations, and edge components of 1/2<111> and <001> mixed dislocations.[27,28] However, in order to activate more slip systems in the 2D columnar structure, the zone axis was chosen as [111] in the present study. Both dislocations with Burges vectors of $1/2[\bar{1}\bar{1}1]$ and [100] have the same edge components of $1/3[\bar{1}\bar{1}2]$ when projected onto [111] plane. So, it is hard to differentiate a $1/2[\bar{1}\bar{1}1]$ dislocation from a [100] dislocation from the projection along [111] zone axis, and it is needed to examine 3D structure of dislocations

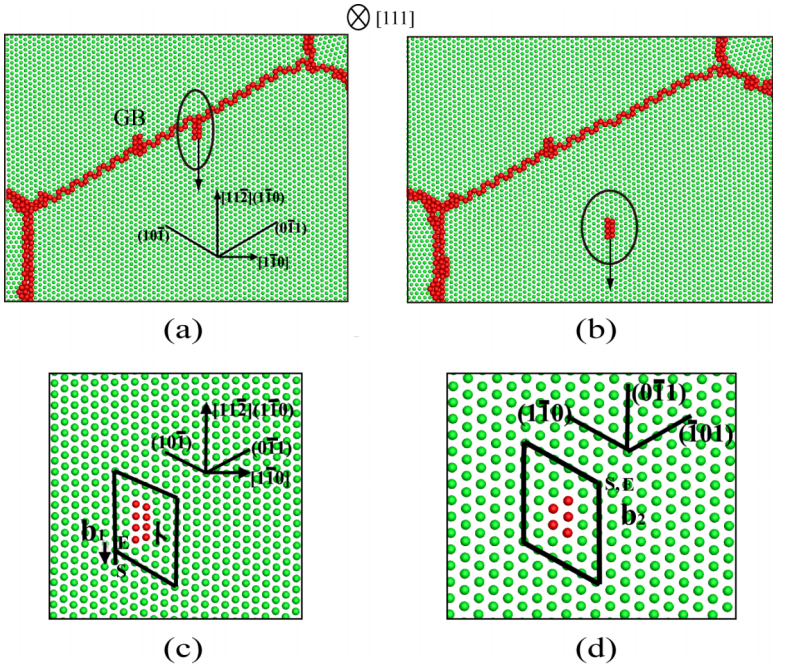

FIG. 5. (a) Nucleation of a dislocation from GBs; (b) Propagation of a dislocation in the interior of grains; (c) A typical edge dislocation ($\vec{b}_1 = 1/2[\bar{1}\bar{1}1]$) with edge component of $1/3[\bar{1}\bar{1}2]$ projected onto [111] plane in the interior of grains; (d) A typical screw dislocation ($\vec{b}_2 = 1/2[111]$) in the interior of grains.

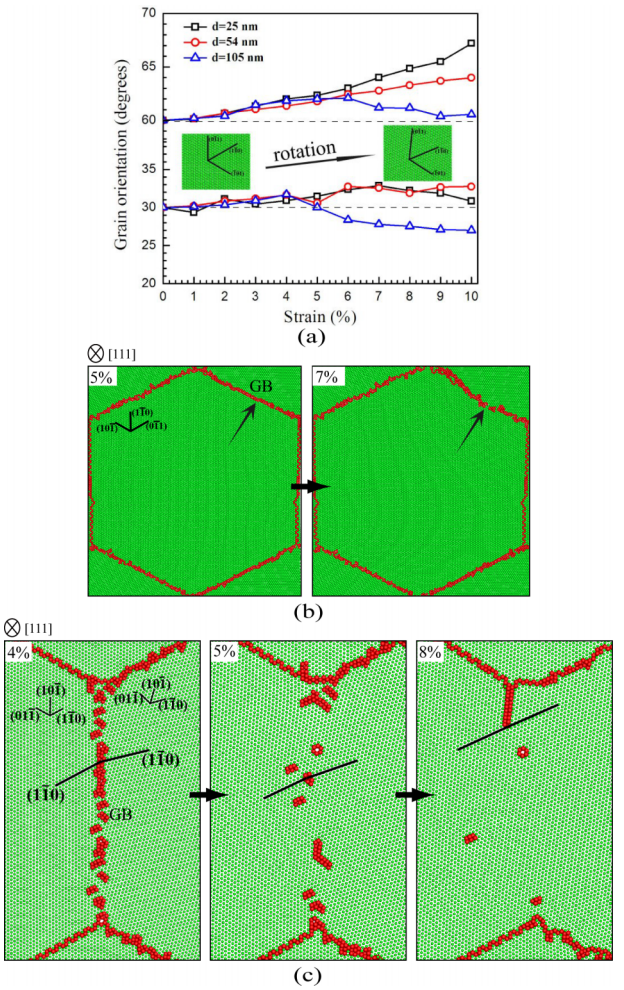

FIG. 6. (a) The grain orientations as a function of tensile strain for selected grains with various grain sizes in the GNG structure; (b) Simulated deformation patterns at 5% and 7% tensile strains in selected 25 nm grains showing GB migration; (c) Simulated deformation patterns at 4%, 5% and 7% tensile strains in selected 25 nm grains showing grain rotation and grain coalescence.

and indentify the dislocation type. The dislocation types were then investigated and can be identified by Burgers circuits and DDA (dislocation detection algorithm) tools in the present study.[43] As shown in Figs 5(c)-5(d), the Burges vector of a screw dislocation is parallel to the dislocation line, while the Burges vector of an edge dislocation is perpendicular to the dislocation line.

Fig. 6(a) shows the grain orientations as a function of tensile strain for selected grains with various grain sizes in the GNG structure. Fig. 6(b) shows simulated deformation patterns at 5% and 7% tensile strains in selected 25 nm grains showing GB migration. Fig. 6(c) shows simulated deformation patterns at 4%, 5% and 7% tensile strains in selected 25 nm grains showing grain rotation and grain coalescence. Based on observations from Fig. 6(a), three conclusions could be drawn as follows: (a) The smaller the grain, the easier for grain rotation when the initial orientation is 60^0; (b) The grain rotations are similar for various grain sizes when the initial orientation is 30^0, which indicates the grain rotations are not only related to grain sizes but also the initial grain orientations; (c) The grain rotations could be clockwise or counter-clockwise. Previous investigations[29,44] also suggest that the GB activities increase with decreasing grain sizes for tens of nm grain size range. A unified approach to four fundamental phenomena associated with GBs and grain growth has recently been formulated: (a) Normal GB motion; (b) Relative translation of the grains parallel to the GB plane coupled to normal GB motion; (c) GB sliding; (d) Grain rotation.[45] This

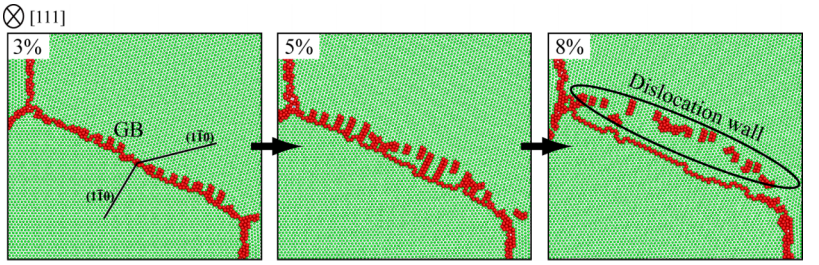

FIG. 7. Simulated deformation patterns at 3%, 5% and 8% tensile strains in selected 54 nm grains showing dislocation nucleation, propagation and formation of dislocation wall near GBs.

indicates that GB motions are generally coupled and curvature driven, which is similar to our observations as indicated in Fig. 6(b). The grain growth mechanisms include GB migration and grain-rotation-induced grain coalescence,[45,46] which are also observed in our simulation for a GB with initial misorientation of 15^0 (Fig. 6(c)). For grains with d = 25 nm in the GNG structure, the deformation mechanisms are dominated by GB migration, grain rotation and grain coalescence although a few dislocations are observed.

Fig. 7 shows simulated deformation patterns at 3%, 5% and 8% tensile strains in selected 54 nm grains showing dislocation nucleation, propagation and formation of dislocation wall near GBs. Based on MD simulations, a transition have been elucidated in deformation mechanisms with decreasing grain size from dislocation-mediated plasticity to GB-associated plasticity in nanocrystalline metals.[29,30,36,39,47] Above "the strongest grain size", the prevailing mechanisms for nanocrystalline metals depend on the stacking-fault energy (SFE), the elastic properties of metals, and the magnitude of the applied stress.[47] The metals with high SFE exhibit a series of loops of perfect dislocations propagating through the grain interiors. By contrast, in the metals with low SFE, complete dislocations could not be nucleated and only partial dislocations could be nucleated from GBs and absorbed by opposite GBs, leaving stacking-fault (SF) behind in the grain interior. In the grains with d = 50 nm in the GNG structure of bcc Fe, perfect dislocations are observed to be nucleated from GBs and propagate to the grain interior, and finally a dislocation wall is formed near GBs (Fig. 7). This dislocation wall can impede further dislocation nucleation and propagation, resulting in strain hardening for the whole structure.

Fig. 8 shows simulated deformation patterns at 3% and 5% tensile strains in selected 105 nm grains showing formation of dislocation wall and dislocation pile-up near GBs. Besides the formation of dislocation wall near GBs, dislocation pile-up is also observed between the initial GB and the newly formed dislocation wall (Fig. 8), which is the first observation by MD simulations to our best knowledge. This dislocation pile-up should contribute significantly to the strain hardening of the whole structure.

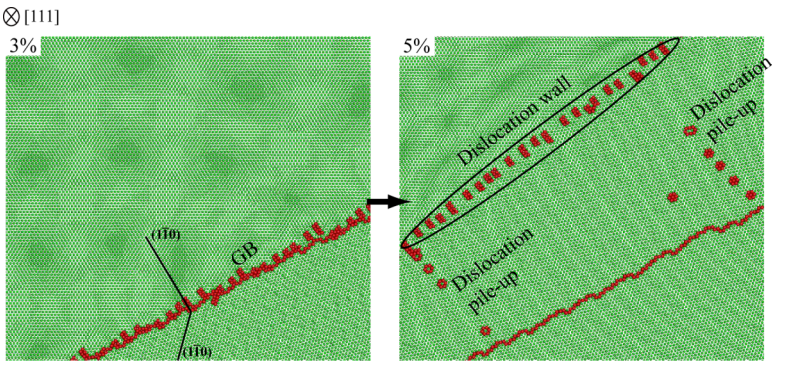

FIG. 8. Simulated deformation patterns at 3% and 5% tensile strains in selected 105 nm grains showing formation of dislocation wall and dislocation pile-up near GBs.

IV. CONCLUDING REMARKS

Large-scale MD simulations have been used to elucidate the atomistic deformation mechanisms of the GNG structure of bcc Fe and the uniform NG structure of bcc Fe in the present study. The grain size gradient in the GNG structure converts the applied uniaxial stress to multi-axial stresses and promotes the dislocation behaviors, thus resulting in extra hardening and slightly higher flow strength when compared to the uniform NG structure even with the stronger grain size. The dominant deformation mechanisms are found to be closely related to the grain sizes in the GNG structure. The deformation mechanisms are dominated by GB activities although few dislocations are observed in the grain interior with d = 25 nm. However, dislocation nucleation from GBs, propagation in the grain interior and formation of dislocation wall near GBs are observed for larger grains (d = 54, 105 nm). Moreover, dislocation pile-up between the newly formed dislocation wall and the initial GBs is observed for grains with d = 105 nm, which is the first observation by MD simulations to our best knowledge. The formation of dislocation wall and dislocation pile-up should contribute significantly to the strain hardening during the plastic deformation. The present findings should provide insights for developing the metals and alloys with superior mechanical properties.

ACKNOWLEDGEMENTS

The financial supports of this work were provided by the National Key Basic Research Program of China (2012CB932203 and 2012CB937500) and NSFC (11222224, 11472286, and 11021262). The simulations reported here were performed at Supercomputing Center of Chinese Academy of Sciences.

[1] H. Gleiter, Prog. Mater. Sci. **33**, 223 (1989).
[2] M. A. Meyers, A. Mishra, and D. J. Benson, Prog. Mater. Sci. **51**, 427 (2006).
[3] R. O. Ritchie, Nature Mater. **10**, 817 (2011).
[4] L. Lu, Y. Shen, X. Chen, L. Qian, and K. Lu, Science **304**, 422 (2004).
[5] L. Lu, X. Chen, X. Huang, and K. Lu, Science **323**, 607 (2009).
[6] K. Lu, L. Lu, and S. Suresh, Science **324**, 349 (2009).
[7] X. Y. Li, Y. J. Wei, L. Lu, K. Lu, and H. J. Gao, Nature **464**, 877 (2010).
[8] Y. H. Zhao, X. Z. Liao, S. Cheng, E. Ma, and Y. T. Zhu, Adv. Mater. **18**, 2280 (2006).
[9] P. V. Liddicoat, X. Z. Liao, Y. H. Zhao, Y. T. Zhu, M. Y. Murashkin, E. J. Lavernia, R. Z. Valiev, and S. P. Ringer, Nature Commun. **1**, 63 (2010).
[10] Y. M. Wang, M. W. Chen, F. H. Zhou, and E. Ma, Nature **419**, 912 (2002).
[11] K. Lu and J. Lu, J. Mater. Sci. Technol. **15**, 193 (1999).
[12] A. Y. Chen, D. F. Li, J. B. Zhang, H. W. Song, and J. Lu, Scripta Mater. **59**, 579 (2008).
[13] T. H. Fang, W. L. Li, N. R. Tao, and K. Lu, Science **331**, 1587 (2011).
[14] X. L. Wu, P. Jiang, L. Chen, F. P. Yuan, and Y. T. Zhu, P. Natl Acad Sci USA **111**, 7197 (2014).
[15] Y. J. Wei, Y. Q. Li, L. C. Zhu, Y. Liu, X. Q. Lei, G. Wang, Y. X. Wu, Z. L. Mi, J. B. Liu, H. T. Wang, and H. J. Gao, Nature Commun. **5**, 3580 (2014).
[16] K. Lu, Science **345**, 1455 (2014).
[17] Y. Xiang, T. Li, Z. Suo, and J. Vlassak, Appl. Phys. Lett. **87**, 161910 (2005).
[18] T. Li and Z. Suo, Inter. J Solids Struc. **43**, 2351 (2006).
[19] Y. M. Wang, E. Ma, and M. W. Chen, Appl. Phys. Lett. **80**, 2395 (2002).
[20] L. Lu, M. L. Sui, and K. Lu, Science **287**, 1463 (2000).
[21] X. L. Wu, Y. T. Zhu, Y. G. Wei, and Q. M. Wei, Phys. Rev. Lett. **103**, 205504 (2009).
[22] X. Feaugas, Acta Mater. **47**, 3617 (1999).
[23] R. J. Asaro, Adv. Appl. Mech. **23**, 1 (1983).
[24] H. Gao, Y. Huang, W. D. Nix, and J. W. Hutchinson, J. Mech. Phys. Solids **47**, 1239 (1999).
[25] X. L. Wu, P. Jiang, L. Chen, J. F. Zhang, F. P. Yuan, and Y. T. Zhu, Mater. Res. Lett. **2**, 185 (2014).
[26] Q. Wei, J. Mater. Sci. **42**, 1709 (2007).
[27] G. M. Cheng, W. W. Jian, W. Z. Xu, H. Yuan, P. C. Millett, and Y. T. Zhu, Maters. Res. Lett. **1**, 26 (2013).
[28] G. M. Cheng, W. Z. Xu, W. W. Jian, H. Yuan, M. H. Tsai, Y. T. Zhu, Y. F. Zhang, and P. C. Millett, J. Mater. Res. **28**, 1820 (2013).
[29] V. Yamakov, D. Wolf, S. R. Phillpot, A. K. Mukherjee, and H. Gleiter, Nature Mater. **1**, 45 (2002).
[30] J. Schiotz and K. W. Jacobsen, Science **301**, 1357 (2003).
[31] H. Van Swygenhoven, P. M. Derlet, and A. G. Froseth, Nature Mater. **3**, 399 (2004).
[32] J. Wang and H. C. Huang, Appl. Phys. Lett. **85**, 5983 (2004).
[33] D. Farkas and B. Hyde, Nano Lett. **5**, 2403 (2005).
[34] A. C. Lund and C. A. Schuh, Acta Mater. **53**, 3193 (2005).
[35] D. Wolf, V. Yamakov, S. R. Phillpot, A. K. Mukherjee, and H. Gleiter, Acta Mater. **53**, 1 (2005).
[36] Z. L. Pan, Y. L. Li, and Q. Wei, Acta Mater. **56**, 3470 (2008).

[37] M. F. Horstemeyer, D. Farkas, S. Kim, T. Tang, and G. Potirniche, Inter. J. Fatigue **32**, 1473 (2010).
[38] T Zhu and J Li, Prog. Mater. Sci. **55**, 710 (2010).
[39] J. B. Jeon, B. Lee, and Y. W. Chang, Scripta Mater. **64**, 494 (2011).
[40] G. Monnet and D. Terentyev, Acta Mater. **57**, 1416 (2009).
[41] A. Spielmannová, A. Machová, and P. Hora, Acta Mater. **57**, 4065 (2009).
[42] M. I. Mendelev, S. Han S, D. J. Srolovitz, G. J. Ackland, D. Y. Sun, and M. Asta, Philosophical Magazine **83**, 3977 (2003).
[43] A. Stukowski and K. Albe, Modell. Simul. Maters. Sci. Eng. **18**, 025016 (2010).
[44] V. Yamakov, D. Moldovan, K. Rastogi, and D. Wolf, Acta Mater. **54**, 4053 (2006).
[45] J. W. Cahn, Y. Mishin, and A. Suzuki, Acta Mater. **54**, 4953 (2006).
[46] D. Moldovan, V. Yamakov, D. Wolf, and S. P. Phillpot, Phys. Rev. Lett. **89**, 206101 (2002).
[47] V. Yamakov, D. Wolf, S. R. Phillpot, A. K. Mukherjee, and H. Gleiter, Nature Mater. **3**, 43 (2004).